

Bistatic Information Fusion for Positioning and Tracking in Integrated Sensing and Communication

Maximilian Bauhofer*, Marcus Henninger†, Thorsten Wild†, Stephan ten Brink*, and Silvio Mandelli†

*University of Stuttgart, 70659 Stuttgart, Germany †Nokia Bell Labs, 70469 Stuttgart, Germany

E-mail: bauhofer@inue.uni-stuttgart.de

Abstract—The distributed nature of cellular networks is one of the main enablers for integrated sensing and communication (ISAC). For target positioning and tracking, making use of bistatic measurements is non-trivial due to their non-linear relationship with Cartesian coordinates. Most of the literature proposes geometric-based methods to determine the target’s location by solving a well-defined set of equations stemming from the available measurements. The error covariance to be used for Bayesian tracking is then derived from local Taylor expansions. In our work we adaptively fuse any subset of bistatic measurements using a maximum likelihood (ML) framework, allowing to incorporate every possible combination of available measurements, i.e., transmitter angle, receiver angle and bistatic range. Moreover, our ML approach is intrinsically flexible, as it can be extended to fuse an arbitrary number of measurements by multistatic setups. Finally, we propose both a fixed and dynamic way to compute the covariance matrix for the position error to be fed to Bayesian tracking techniques, like a Kalman filter. Numerical evaluations with realistic cellular communications parameters at mmWave frequencies show that our proposal outperforms the considered baselines, achieving a location and velocity root mean square error of 0.25 m and 0.83 m/s, respectively.

Index Terms—Bistatic, positioning, tracking, integrated sensing and communication (ISAC).

I. INTRODUCTION

Integrated sensing and communication (ISAC) is expected to be one of the main novel features of future cellular communication standards. It equips the network with the ability to acquire knowledge about its surrounding environment, enabling new services [1]. The plethora of applications include detection and localization of pedestrians and automated guided vehicles (AGV) in factories, mobile handover prediction, SLAM and digital twins [2].

Those use cases require positioning not only of actively transmitting terminals – which has been available since at least 4G [3] – but also in a radar-like, passive manner through backscattering only. To enable this, the respective measures have to be extracted from the communications signal [4] and can then be fused for positioning a target [5]. In addition, one would like to have the capability to track objects over time.

While there is some work on tracking for general radar applications, literature on distributed cellular based tracking is sparse. The addition of sensing on top of legacy communication services imposes constraints by the cellular system, which

was not designed with this task in mind. Resulting limitations, regulations and backwards compatibility with older standards have to be taken into account. Further, in contrast to typical radar setups, potential targets can appear in close proximity to the system. For tracking itself, prior art suggests to operate directly with the received signal [6], [7] leveraging the synergy of detection and tracking. However, factors like multiple targets, bistatic operations, complexity, or the large signaling overhead to a central entity render this approach impractical in current systems. Based on subspace tracking [8], the authors of [9] propose a low complexity method combining angle-of-departure (AoD) and angle-of-arrival (AoA) together with ESPRIT. In contrast to this, the approach of extracting the target measurements in a first step and then applying tracking is largely suggested by radar literature [10]. However, this requires linearizing the non-Cartesian measurements, which is typically done by extended or unscented Kalman filters (KFs) [11], [12]. More recent work [13] and an earlier study [14] suggest that a linear KF, fed with measurements fused to location estimates, results in better performance, known as converted measurement KF. The necessary measurement error covariance matrix of such an estimate can be approximated by linearization through a low-order Taylor series.

In this work, we leverage an maximum likelihood (ML) approach for probabilistically fused position estimates. We derive the corresponding covariance dynamically from the fusion Hessian matrix. Both are then fed to a linear KF. This approach can be seen as an extension to the state of the art, with equal performance but more versatile applications, as it can fuse an arbitrary number of measurements. A second, less complex but even more powerful approach uses the same ML location estimate with a position-independent fixed covariance based on prior calibration with the expected root mean square error (RMSE). Their main advantage is easy expandability to multistatic scenarios in which measurements from different sensor pairs are combined. In our 2D campus network simulations, we use bistatic range, AoD, and AoA for a single target tracking task. Our main contributions are:

- 1) We derive an ML approach to fuse the bistatic information (range, transmit and receive angle) or subsets thereof to localize a target.
- 2) We show the similarities of our ML approach and state of the art, and the superior performance of the fixed covariance approach, which are both more versatile than

This work has been submitted to the IEEE for possible publication. Copyright may be transferred without notice, after which this version may no longer be accessible.

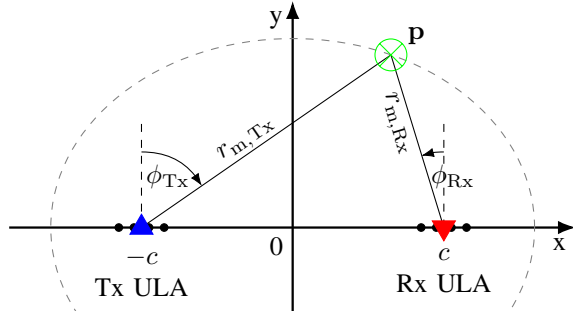


Fig. 1: Schematic of a bistatic ISAC system. Tx and Rx ULA are placed at $\pm c$ from the origin in x-direction. The target at location \mathbf{p} is marked with its geometrically derived quantities r_b , ϕ_{Tx} , ϕ_{Rx} , for bistatic range, AoD at Tx, and AoA at Rx, respectively.

the baseline and enhance the performance of KFs.

- 3) We compare our proposals to the baseline technique with numerical evaluations based on realistic cellular system parametrization and complex target trajectories.

II. SYSTEM MODEL

We consider the bistatic two-dimensional system depicted in Fig. 1. The transmitter (Tx) and receiver (Rx) uniform linear arrays (ULAs) are positioned on the x-axis at $\mathbf{p}_{Tx} = [-c, 0]^T$, $\mathbf{p}_{Rx} = [+c, 0]^T$, respectively. From bistatic geometry, the baseline is therefore $2c$, corresponding to half the linear eccentricity for the isorange ellipse with Tx and Rx in its foci. We describe an impulsively scattering target by its state $\boldsymbol{\theta} = [\mathbf{p}, \mathbf{v}]^T$, with location $\mathbf{p} = [p_x, p_y]^T$ and velocity $\mathbf{v} = [v_x, v_y]^T$. We define the bistatic range $r_b = r_{m,Tx} + r_{m,Rx}$, AoD ϕ_{Tx} , and AoA ϕ_{Rx} as

$$r_b(\mathbf{p}) = \|\mathbf{p} - \mathbf{p}_{Tx}\|_2 + \|\mathbf{p} - \mathbf{p}_{Rx}\|_2 \quad (1)$$

$$= \sqrt{(p_x + c)^2 + p_y^2} + \sqrt{(p_x - c)^2 + p_y^2},$$

$$\phi_{Tx}(\mathbf{p}) = -\arctan\left(\frac{p_x + c}{|p_y|}\right), \quad (2)$$

$$\phi_{Rx}(\mathbf{p}) = -\arctan\left(\frac{p_x - c}{|p_y|}\right). \quad (3)$$

The measured angles at the arrays are expressed using the normalized angular frequency (NAF) [15] given as

$$\eta(\phi) = \frac{d}{\lambda_c} \sin(\phi), \quad (4)$$

with ULA element distance d and carrier wavelength λ_c .

The bistatic setup acquires range and angular measurements with additive white Gaussian noise (AWGN) denoted as $\alpha_r \sim \mathcal{N}(0, \sigma_r^2)$, $\alpha_{\eta_{Tx}}, \alpha_{\eta_{Rx}} \sim \mathcal{N}(0, \sigma_\eta^2)$, respectively. This yields the measurements

$$\tilde{r}_b = r_b + \alpha_r \quad (5)$$

$$\tilde{\eta}_{Tx} = \eta(\phi_{Tx}) + \alpha_{\eta_{Tx}}, \quad (6)$$

$$\tilde{\eta}_{Rx} = \eta(\phi_{Rx}) + \alpha_{\eta_{Rx}}, \quad (7)$$

where the dependency on \mathbf{p} has been dropped for readability.

III. BISTATIC POSITIONING

In this section we want to estimate the Cartesian location of a target from the available measurements (5), (7) in the system. A single measurement will lead to an underdetermined system, from which an unambiguous target location cannot be deduced. For exactly two measurements a precise location can be derived with prior art geometric-based approaches, which are described in the first subsection. The second subsection introduces our probabilistic approach, which can even handle an overdetermined system where all three measures are available. With both approaches we describe also how to estimate the location error's covariance matrix, which indicates a confidence in the derived position to be used for target tracking with Bayesian tracking techniques.

A. Geometric Positioning

In geometric positioning, exactly two values among range, AoD, and AoA need to be combined to determine the target location. Combining the two angles, AoD and AoA, yields the following conversion function to Cartesian coordinates

$$\mathbf{p}(\eta_{Tx}, \eta_{Rx}) = \begin{bmatrix} -c \frac{\tan(\phi(\eta=\eta_{Rx})) + \tan(\phi(\eta=\eta_{Tx}))}{\tan(\phi(\eta=\eta_{Rx})) - \tan(\phi(\eta=\eta_{Tx}))} \\ \frac{2c}{\tan(\phi(\eta=\eta_{Rx})) - \tan(\phi(\eta=\eta_{Tx}))} \end{bmatrix}, \quad (8)$$

computed by inverting (4). The other combination of a single angle, AoD or AoA, with bistatic range requires a conversion to the respective ULA-centric monostatic range

$$r_m(\phi', r_b) = \frac{r_b^2 - 4c^2}{2(r_b - 2c \sin(\phi'))}, \quad (9)$$

with $\phi' = \pi + \phi(\eta_{Tx})$ or $\phi' = \phi(\eta_{Rx})$ for Tx or Rx measurement, respectively. The final Cartesian location is obtained by a coordinate transform and translation

$$\mathbf{p}(r_m, \eta, c) = \begin{bmatrix} -r_m \sin(\phi(\eta)) \mp c \\ r_m \cos(\phi(\eta)) \end{bmatrix}. \quad (10)$$

For the respective estimation covariance matrix, we employ the first-order Taylor series expansion approach by [14]. The components of the estimated location $\hat{\mathbf{p}} = \mathbf{p}(\tilde{\mathbf{m}})$ can be deduced from the noisy measurements vector $\tilde{\mathbf{m}}$ and the proper conversion function components $p_i(\cdot)$ among (8) or (9). Accordingly, we write the Taylor expansion of $\mathbf{p}(\tilde{\mathbf{m}})$ around $\tilde{\mathbf{m}}$, keeping only the first-order components as follows

$$\hat{p}_i = p_i(\tilde{\mathbf{m}}) = p_i(\mathbf{m}) + \sum_{j=1}^2 \frac{\partial p_i(\mathbf{m})}{\partial m_j} \alpha_j. \quad (11)$$

Assuming zero-mean AWGN, we have $\mathbb{E}[\alpha_j] = 0$, thus $\mathbb{E}[\hat{p}_i] = p_i(\mathbf{m})$ and therefore variance $\mathbb{E}[[\alpha_j]^2] = \sigma_j^2$. From this, the elements of the converted error covariance matrix, here $\hat{\mathbf{C}}_{\text{Geo}}^{2 \times 2}(\tilde{\mathbf{m}})$, approximating the confidence from measurement to Cartesian space, are

$$\begin{aligned} [\mathbf{C}_{\text{Geo}}(\mathbf{m})]_{pq} &= \mathbb{E} \left[\sum_{j=1}^2 \frac{\partial p_p(\mathbf{m})}{\partial m_j} \alpha_j \sum_{j=1}^2 \frac{\partial p_q(\mathbf{m})}{\partial m_j} \alpha_j \right] \\ &\approx \left[\hat{\mathbf{C}}_{\text{Geo}}(\tilde{\mathbf{m}}) \right]_{pq} = \sum_{j=1}^2 \frac{\partial p_p(\tilde{\mathbf{m}})}{\partial m_j} \frac{\partial p_q(\tilde{\mathbf{m}})}{\partial m_j} \sigma_j^2. \end{aligned} \quad (12)$$

Note that in [14] the Taylor expansion was considered up to the second order, since it was proven to be necessary at high distance from Tx and Rx. In our study, for the sake of simplicity and due to the short range applications we target, we limit ourselves to the first order.

B. Maximum Likelihood Positioning

In this subsection we derive how to fuse the available measurements and estimate the target location with a ML approach. We define the likelihood function for the target position, given o available noisy observations stacked in $\tilde{\mathbf{m}}$ as

$$\mathcal{L}(\tilde{\mathbf{m}}|\mathbf{p}) = \frac{\exp\left(-\frac{1}{2}(\mathbf{f}(\mathbf{p}) - \tilde{\mathbf{m}})^\top \mathbf{C}^{-1}(\mathbf{f}(\mathbf{p}) - \tilde{\mathbf{m}})\right)}{\sqrt{(2\pi)^o \det(\mathbf{C})}}, \quad (13)$$

where the basis is the multivariate normal distribution due to the assumed AWGN in the measurements, according to (5) – (7). The variances of the available measurements form the diagonal covariance matrix \mathbf{C} . The vector-function $\mathbf{f}(\mathbf{p})$ converts a candidate location \mathbf{p} into the space of available measurements according to (1) – (4). The ML estimate is then

$$\begin{aligned} \hat{\mathbf{p}}_{\text{ML}} &= \arg \max_{\mathbf{p}} (\ln(\mathcal{L}(\tilde{\mathbf{m}}|\mathbf{p}))) \\ &= \arg \min_{\mathbf{p}} ([\mathbf{f}(\mathbf{p}) - \tilde{\mathbf{m}}]^\top \mathbf{C}^{-1} [\mathbf{f}(\mathbf{p}) - \tilde{\mathbf{m}}]). \end{aligned} \quad (14)$$

The error covariance matrix of the location estimate to be fed to Bayesian tracking algorithms is computed as the inverted negative Hessian matrix $\hat{\mathbf{C}}_{\text{ML}} = -\hat{\mathbf{H}}_{\text{ML}}^{-1}$ of the log-likelihood function [16]

$$[\hat{\mathbf{H}}_{\text{ML}}]_{pq} = \frac{\partial^2 \ln(\mathcal{L}(\tilde{\mathbf{m}}|\mathbf{p}))}{\partial \tilde{m}_p \partial \tilde{m}_q}. \quad (15)$$

Note that this probabilistic approach can estimate – starting from two different measurement types – also overdetermined systems with an arbitrary number of measurements. This can also be leveraged for fusing measurements from multistatic setups with, for example, multiple receivers, by selecting the vector-conversion function $\mathbf{f}(\mathbf{p})$ appropriately.

As an alternative, one can assume a fixed hand-tuned location error covariance matrix. In our numerical study we consider a diagonal matrix, i.e., assume no correlation between x- and y-coordinate

$$\hat{\mathbf{C}}_{\text{fix}} = \text{diag}(\sigma_x^2, \sigma_y^2) = \begin{bmatrix} \sigma_x^2 & 0 \\ 0 & \sigma_y^2 \end{bmatrix}. \quad (16)$$

This “fixed” approach is computationally simple, not requiring any matrix inversion upon each ML location estimation.

IV. KALMAN FILTER BASED TRACKING

Measurements acquired over time, while the target moves, can be fused with Bayesian tracking techniques. In this work we input the location – and corresponding error covariance estimates – to a KF. Its linear dynamic system model is

$$\boldsymbol{\theta}[n] = \mathbf{A} \cdot \boldsymbol{\theta}[n-1] + \boldsymbol{\beta}[n] \quad (17)$$

with state $\boldsymbol{\theta} = [p_x, p_y, v_x, v_y]^\top$ for each discrete time instance n . We assume a constant velocity physical prediction model

$$\mathbf{A} = \begin{bmatrix} 1 & 0 & \Delta t & 0 \\ 0 & 1 & 0 & \Delta t \\ 0 & 0 & 1 & 0 \\ 0 & 0 & 0 & 1 \end{bmatrix}. \quad (18)$$

Given the sufficiently high update rate likely to be available in ISAC systems [17], combined with limited acceleration, the process noise realizations $\boldsymbol{\beta}[n]$ remain small, justifying the adoption of the constant velocity model (17), (18). The measurement model includes the location estimates $\hat{\mathbf{p}}$ from (8), (9), or (14), with the error covariance $\hat{\mathbf{C}}$ either fixed (16) or dynamically computed from (12) or (15). For the well-known KF prediction and update equations, refer, e.g., to [18].

V. RESULTS

This section discusses the simulation setup and the results for positioning and tracking based on numerical evaluations.

A. Simulation Setup

For the bistatic system, we assume that Tx and Rx are perfectly synchronized. Further, we consider a single impulsively scattering target, such that matching targets to measurements is not necessary. Based on single set of measurements processing, we work with perfect ground truth and refer to [4], [5] for details on how these would be extracted from, e.g., an orthogonal frequency-division multiplexing (OFDM) transmission. While we limit ourselves to the 2D case, 3D should be a straightforward extension of the respective equations. We follow [1] for the system parameters, with an update rate of 10 ms and noise parameters $\sigma_r = 0.15$ m and $\sigma_\eta = 0.022$, equivalent to 4° in boresight. Given our indoor focus, the baseline (i.e., Tx-Rx distance) is selected to be $2c = 10$ m.

For angle-only positioning, we discard realizations which would result in a location estimate behind the baseline, i.e., $y < 0$. The sample locations have a minimum distance of 5 m to the baseline. For ML fusion, estimates are restricted to $y > 0$. The initial guess is located in a random location up to 3 m from the ground truth location, which in reality can be obtained using the predicted state from the tracker. For tracking, position estimates are discarded if they are further than 8 m away from the previously updated state. Except for tracking based on AoD+AoA position estimates, we have not enabled any filter reset. For the two angles case a reset is necessary due to the large position estimation variations, i.e., if there was (i) no state update for the last 0.5 s, or (ii) the state update lies far outside the evaluated area. For simplicity, the tracker is initialized and reset with the ground truth state and initial error covariance $\text{diag}(0.01, 0.01, 0.01, 0.01)$. Tests with initialization based on the first location estimate with zero velocity showed convergence in around 1 s with negligible RMSE loss over a 60 s long track duration. The Kalman filter process noise is empirically set to $\text{diag}(0.3, 0.3, 0.3, 0.3)$. Regarding the measurement covariance matrix to be input to the KF, we evaluate different proposals. All geometric

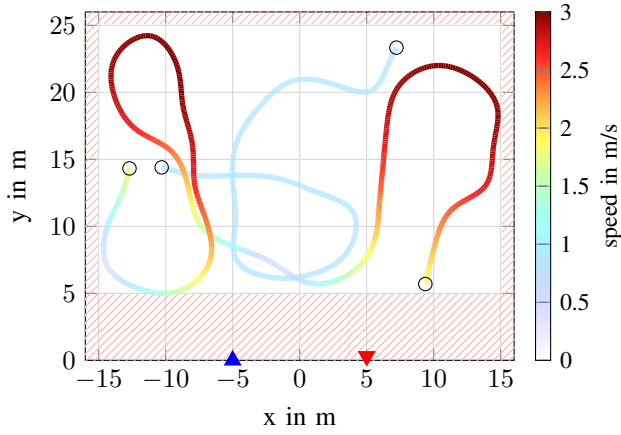


Fig. 2: Two exemplary trajectories with 60 s duration used for tracker evaluation.

based approaches are computed according to (12). For the ML localization, we propose two variants. First, the explicit Hessian according to (15), derived analytically in Appendix A, as we have seen slight performance improvements compared to numerical approximations. As an alternative, we evaluate the computationally simple “fixed” covariance matrix baseline (16). In this approach the diagonal variances are the squared RMSEs of the position estimation evaluation in Tab. I.

For positioning evaluation, we draw 5000 samples from each point on a 10×10 uniform grid, bounded by $x \in [-15, 15]$ m and $y \in [5, 35]$ m. For tracking evaluation, every location estimator is run on 120 tracks, with 40 trials on each. Fig. 2 exemplarily depicts two such trajectories. The track generation follows a pseudorandom walk starting from a random point in the white area shown in Fig. 2. Random change of directions will then generate a series of points, interpolated with cubic-Bezier curves. The speed profile is generated according to a sinusoidal waveform of random initial phase, period lengths of $\{30, 70, 100, 1e8\}$ s, with minimum and maximum values of 0.5 and 3 m/s, respectively, for a duration of 60 s.

Evaluation is based on the mean absolute error and RMSE between estimates and ground truth

$$\text{RMSE} = \sqrt{\mathbb{E}[\|\mathbf{x} - \hat{\mathbf{x}}\|_2^2]}, \quad (19)$$

where \mathbf{x} is either location \mathbf{p} or velocity \mathbf{v} .

From Fig. 3, we observe a number of peculiarities when working with ULAs. The left figure shows the difference in angle distribution from NAF to radiant domain. The upper NAF image depicts the histogram for three distinct incident angles in red after adding noise with constant variance. Transforming this into the radiant domain in the lower left using the non-linear trigonometric function in (4) reveals a broadening of the distribution away from boresight. From this relation, the Gaussian noise distribution also changes its shape. In both images, the light blue distribution showcases the ULA property of angular wrapping (i.e., periodicity) around $\pm 90^\circ$. A similar behavior can be observed in the right figure, which

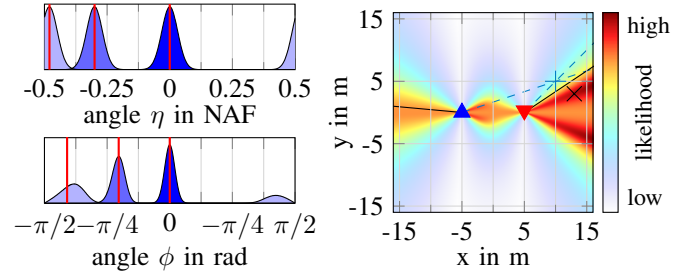


Fig. 3: ULA and NAF peculiarities. (left) Histogram for three distinct noisy incident angles with constant variance in NAF and its influence on the radiant domain. (right) ML heatmap of an estimated target location (\times), based on noisy AoD and AoA measurements (—) from its ground-truth location (+).

depicts the likelihood value of every location given two noisy angle measurements. Again, the periodic angle behavior can be observed from the transmitter angle wrapped to the other side. A 1D ULA cannot distinguish the responses from frontside and backside, resulting in a mirror behavior around $y = 0$. The ML estimate follows this property with a relatively high likelihood for locations $x < -5$ m. Note that the constant likelihood on the baseline between Tx and Rx, where measured angles do not intersect but overlap with constant range measurements, is consistent with bistatic radar theory.

B. Location Estimation

For location estimation, Fig. 4 shows a selection of the distribution of location estimates from different fusion types. In the cropped left image, we can observe the fanning-out of estimates for the fusion of AoD and AoA, irrespective of the approach. This results in almost unbounded location estimates for $\eta_{\text{Tx}} \approx \eta_{\text{Rx}}$. In the center image, substituting one angle with bistatic range significantly lowers the sample spread, resulting in a contact lens shaped distribution well-known from bistatic radar. The estimates are now asymmetrically distributed with lower variance around the observing ULA. The same figure but for the geometric positioning approach would reveal angles reappearing on the other side, as described in Fig. 3. The right image combines all measurements, which is only possible for the ML approach, resulting in a symmetric image with the

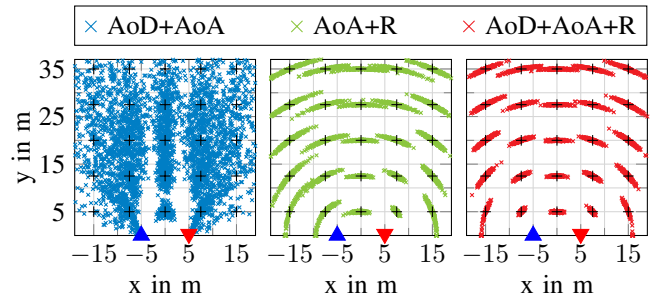


Fig. 4: Distribution of location estimates from ML fusion of different measurements. For the sake of overview, only a 5×5 sample grid with 154 realizations per point is plotted.

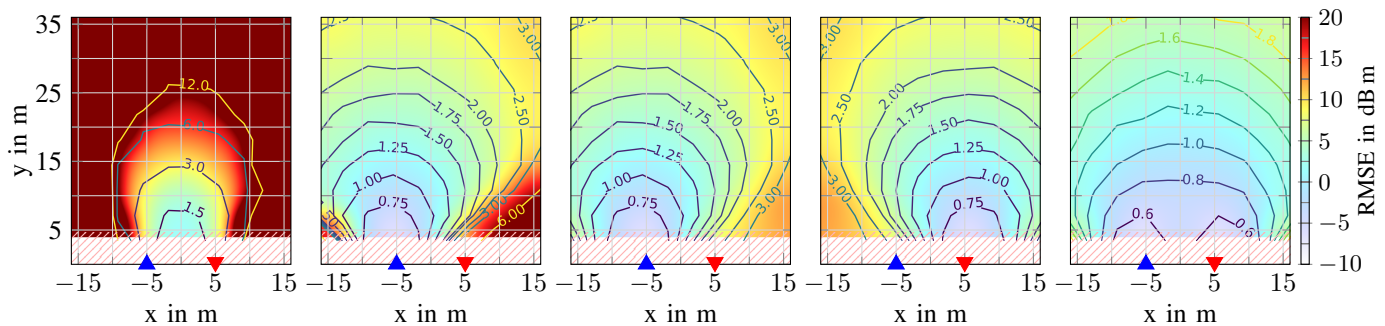


Fig. 5: Exemplary positioning RMSE distribution for a 30×35 m scenario using different approaches and combined measurements. (1) ML AoD+ AoA, (2) geometric AoD+range, (3) ML AoD+range, (4) ML AoA+range, (5) ML AoD+ AoA+range. The heatmap is based on the 10×10 grid with bicubic interpolation between points in decibel and contours in absolute scale.

lowest sample spread. The conversion of these samples to location RMSE heatmaps is shown in Fig. 5. Geometric and ML approach show equal performance for two angles. For a single angle with range (Figs. 5.2 and 5.3) there is a slight improvement for the latter in areas close to the baseline, arising from the described angle continuity. Figs. 5.3 and 5.4 show that a change of measured angle just mirrors the asymmetrical image. In general, locations closer to the angle observing ULA yield lower variance due to the low angular spread. To quantify the performance, Tab. I provides the respective RMSEs averaged over the trajectory area, also used in the fixed covariance baseline tracker.

TABLE I: ML position estimation RMSE performance, average of points within $x \in [-15, 15]$ m and $y \in [-5, 25]$ m.

Quantity	AoD+ AoA	AoD+R	AoA+R	AoD+ AoA+R
x in m	353.72	1.44	1.44	0.9
y in m	90.71	0.99	0.98	0.53
$\ \cdot\ _2$ in m	371.68	1.85	1.84	1.1

The dotted position error cumulative distribution function (CDF) curves in Fig. 6 confirm these results for later comparison with tracking. We plot ML only, with the geometric approach slightly degrading at the high percentiles for fusion of one angle and range. Here, due to the symmetric sample points, the chosen angle is irrelevant. Overall, using the overdetermined system – incorporating a range measurement on top of two angles – we see a decrease of 46%, resulting in a mean absolute position error of 2.32 m for the 95th percentile.

C. Tracking Performance

Running the tracking algorithms, the solid and dashed lines in Fig. 6 show the location performance for the assumed fixed covariance matrix and our ML approach, respectively. We omit the curves for state of the art tracking by geometric positioning as they overlap with (---, -.-). Overall, tracking improves the positioning error by 57 – 82%. In our scenario, tracking with a position-independent “Fixed” covariance matrix does not only outperform the state of the art baseline, but also

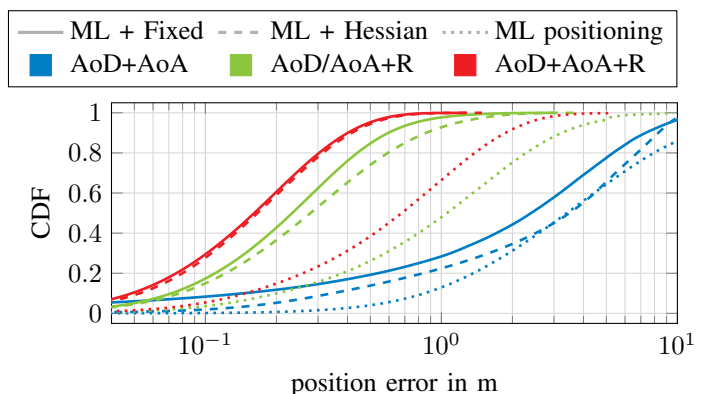


Fig. 6: CDFs of the expected error for positioning only and tracking with KF with the Fixed and Hessian approaches. The evaluated area is $x \in [-15, 15]$ m and $y \in [-5, 25]$ m.

the Hessian-based approach. This suggests that the tracker adheres too strongly to the measurements with lower trust in its predicted state. We observed that the approaches relying on the Hessian and the Taylor approximation used in the geometric results follow this trend. These capture the strong non-Gaussian/elliptical contact lens shaped distribution away from boresight. We conclude that using prior information, e.g., through measurements, is beneficial for tracking for this use case and also reduces the computational load. Tab. II shows the detailed averaged results for tracking. Coherent with the results on positioning, we see that – compared to just using angles – incorporating a range measurement is beneficial. The combination of our ML proposal together with a sample

TABLE II: Tracker RMSE performance

Est. Method	Quantity	AoD+ AoA	AoD+R	AoA+R	AoD+ AoA+R
Geometric	Location in m	4.8	0.56	0.53	n.a.
	Velocity in m/s	1.19	0.89	0.88	n.a.
ML - Hessian	Location in m	4.8	0.56	0.53	0.26
	Velocity in m/s	1.19	0.89	0.88	0.81
ML - Fixed	Location in m	4.21	0.4	0.38	0.25
	Velocity in m/s	1.63	0.9	0.9	0.83

based fixed covariance leads to a more consistent tracker due to a better error covariance estimate. Especially when combining all measurements and mainly boresight targets, the Hessian-based covariance might be an option with almost no positioning degradation, slightly better velocity estimation and no need for pre-processing/sampling the scenario for the values in Tab. I. Again, this performance is further enhanced by incorporating all available measurements, which is only possible with our “ML - Fixed” approach, resulting in a location RMSE down to 0.25 m. We observe the same behavior for the velocity estimate, although higher in magnitude. This relatively high error results from the high accelerations and should be lower in real-world trajectories.

VI. CONCLUSION

In this paper, we have presented a versatile ML approach for the fusion of bistatic measurements into a target location estimate. We demonstrated its performance with 2D numerical evaluations based on an ISAC system parametrization for an indoor scenario with a single target on complex trajectories. The combination of our approach with a linear KF outperforms current state of the art geometric based techniques with respect to tracking performance by 53% and 6%, for a location and velocity RMSE of 0.25 m and 0.83 m/s, respectively. In addition, we showcased the sub-optimality of approaches relying on Taylor approximation or Hessian to compute the localization error covariance and proposed a superior heuristic with even lower complexity. Another benefit of this probabilistic method is the possibility of combining an arbitrary number of combined measurements, enabling multistatic setups with multiple Tx and/or Rx. Incorporating also Doppler information, extension to 3D multi-target capabilities with target-to-measurement association and validation with measurements are topics for future work.

ACKNOWLEDGMENTS

The authors would like to thank Alexander Felix for his valuable feedback during the development of this work.

This work was developed within the KOMSENS-6G project, partly funded by the German Ministry of Education and Research under grant 16KISK112K.

APPENDIX A

DERIVATIONS FOR ANALYTICAL HESSIAN MATRICES

To derive the Hessian respectively location error covariance matrices, we use (15) and feed the respective log-likelihood function from (13). Depending on the fusion type with different $\tilde{\mathbf{m}}$, Tab. III lists the variables assuming no correlation between the measurement types.

TABLE III: Variables for analytical Hessian and Jacobian matrix of ML approach from (13).

Fusion Type	Measurement Vector	Measurement Covariance
AoD+AoA	$\tilde{\mathbf{m}} = [\tilde{\eta}_{Tx}, \tilde{\eta}_{Rx}]^T$	$\mathbf{C} = \text{diag}(\sigma_{\eta}^2, \sigma_{\eta}^2)$
AoD+R	$\tilde{\mathbf{m}} = [\tilde{\eta}_{Tx}, \tilde{r}_b]^T$	$\mathbf{C} = \text{diag}(\sigma_{\eta}^2, \sigma_r^2)$
AoA+R	$\tilde{\mathbf{m}} = [\tilde{\eta}_{Rx}, \tilde{r}_b]^T$	$\mathbf{C} = \text{diag}(\sigma_{\eta}^2, \sigma_r^2)$
AoD+AoA+R	$\tilde{\mathbf{m}} = [\tilde{\eta}_{Tx}, \tilde{\eta}_{Rx}, \tilde{r}_b]^T$	$\mathbf{C} = \text{diag}(\sigma_{\eta}^2, \sigma_{\eta}^2, \sigma_r^2)$

From (1) – (4), the corresponding conversion function $\mathbf{f}(\mathbf{p})$ for (13) is then a combination of

$$\begin{aligned}
 f_{r_b}(\mathbf{p}) &= \sqrt{(p_x + c)^2 + p_y^2} + \sqrt{(p_x - c)^2 + p_y^2}, \\
 f_{\eta_{Tx}}(\mathbf{p}) &= -\frac{d}{\lambda} \sin\left(\arctan\left(\frac{p_x + c}{p_y}\right)\right), \quad p_y > 0, \\
 f_{\eta_{Rx}}(\mathbf{p}) &= -\frac{d}{\lambda} \sin\left(\arctan\left(\frac{p_x - c}{p_y}\right)\right), \quad p_y > 0.
 \end{aligned}$$

REFERENCES

- [1] S. Mandelli, M. Henninger, M. Bauhofer, and T. Wild, “Survey on Integrated Sensing and Communication Performance Modeling and Use Cases Feasibility,” in *2023 2nd Int. Conf. on 6G Networking (6GNet)*, Oct. 2023, pp. 1–8.
- [2] F. Liu *et al.*, “Integrated Sensing and Communications: Toward Dual-Functional Wireless Networks for 6G and Beyond,” *IEEE J. on Sel. Areas in Commun.*, vol. 40, no. 6, pp. 1728–1767, Mar. 2022.
- [3] 3GPP, “Evolved Universal Terrestrial Radio Access (E-UTRA); LTE Positioning Protocol (LPP);” Technical Specification Group RAN, TS 36.355, 2022, Version 17.0.0.
- [4] K. M. Braun, “OFDM Radar Algorithms in Mobile Communication Networks,” Ph.D. dissertation, Karlsruher Institut für Technologie (KIT), 2014.
- [5] M. Bauhofer, S. Mandelli, M. Henninger, T. Wild, and S. ten Brink, “Multi-Target Localization in Multi-Static Integrated Sensing and Communication Deployments,” in *2023 2nd Int. Conf. on 6G Networking (6GNet)*, 2023, pp. 1–4.
- [6] S. Davey, M. Rutten, and B. Cheung, “A comparison of detection performance for several Track-Before-Detect algorithms,” in *2008 11th Int. Conf. on Inf. Fusion*, 2008, pp. 1–8.
- [7] R. Lu, X. Liu, and X. Chen, “Localization and tracking of multiple fast moving targets in bistatic MIMO radar,” *Signal Process.*, vol. 203, p. 108780, Feb. 2023.
- [8] B. Yang, “Projection approximation subspace tracking,” *IEEE Trans. on Signal Process.*, vol. 43, no. 1, pp. 95–107, Jan. 1995.
- [9] H. Wu and X. Zhang, “DOD and DOA tracking algorithm for bistatic MIMO radar using PASTD without additional angles pairing,” in *IEEE Fifth Int. Conf. on Adv. Comput. Intell. (ICACI)*, 2012, pp. 1132–1136.
- [10] D. Lerro and Y. Bar-Shalom, “Tracking with debiased consistent converted measurements versus EKF,” *IEEE Trans. on Aerospace and Electron. Syst.*, vol. 29, no. 3, pp. 1015–1022, Jul. 1993.
- [11] D. F. Crouse, “One can do better than the unscented Kalman filter for multistatic tracking,” in *2013 IEEE Aerospace Conf.*, 2013, pp. 1–20.
- [12] R. A. Coogle, L. D. Smith, and W. D. Blair, “Mitigating the bias in converted bistatic radar measurements using the unscented transform,” in *2013 IEEE Aerospace Conf.*, 2013, pp. 1–7.
- [13] H. Marom, Y. Bar-Shalom, and B. Milgrom, “Bistatic radar tracking with significantly improved bistatic range accuracy,” *IEEE Trans. on Aerospace and Electronic Systems*, vol. 59, no. 1, pp. 52–62, Feb. 2023.
- [14] X. Tian and Y. Bar-Shalom, “Coordinate Conversion and Tracking for Very Long Range Radars,” *IEEE Trans. on Aerospace and Electronic Systems*, vol. 45, no. 3, pp. 1073–1088, Jul. 2009.
- [15] S. Mandelli, M. Henninger, and J. Du, “Sampling and Reconstructing Angular Domains With Uniform Arrays,” *IEEE Trans. on Wireless Commun.*, vol. 22, no. 6, pp. 3628–3642, Jun. 2023.
- [16] W. C. Thacker, “The role of the hessian matrix in fitting models to measurements,” *Journal of Geophysical Research: Oceans*, vol. 94, no. C5, pp. 6177–6196, May 1989.
- [17] T. Wild, A. Grudnitsky, S. Mandelli, M. Henninger, J. Guan, and F. Schaich, “6G Integrated Sensing and Communication: From Vision to Realization,” in *20th Eur. Radar Conf. (EuRAD)*, 2023, pp. 355–358.
- [18] U. Spagnolini, *Statistical Signal Processing in Engineering*. Hoboken, NJ, USA: John Wiley & Sons, 2018.